

Amplitude and Phase of Wave Packets in a Linear Potential

Georgi Gary Rozenman,^{1,2} Matthias Zimmermann,³ Maxim A. Efremov,³
Wolfgang P. Schleich,^{3,4} Lev Shemer,⁵ and Ady Arie²

¹Raymond and Beverly Sackler School of Physics & Astronomy, Faculty of Exact Sciences, Tel Aviv University, Tel Aviv 69978, Israel

²School of Electrical Engineering, Iby and Aladar Fleischman Faculty of Engineering, Tel Aviv University, Tel Aviv 69978, Israel

³Institut für Quantenphysik and Center for Integrated Quantum Science and Technology (IQST), Universität Ulm, 89081 Ulm, Germany

⁴Hagler Institute for Advanced Study at Texas A & M University, Texas A & M AgriLife Research,

Institute for Quantum Science and Engineering (IQSE), and Department of Physics and Astronomy, Texas A & M University,
College Station, Texas 77843-4242, USA

⁵School of Mechanical Engineering, Faculty of Engineering, Tel Aviv University, Tel Aviv 69978, Israel



(Received 24 July 2018; published 28 March 2019)

We theoretically study and successfully observe the evolution of Gaussian and Airy surface gravity water wave packets propagating in an effective linear potential. This potential results from a homogeneous and time-dependent flow created by a computer-controlled water pump. For both wave packets we measure the amplitudes *and* the cubic phases appearing due to the linear potential. Furthermore, we demonstrate that the self-acceleration of the Airy surface gravity water wave packets can be completely canceled by a linear potential.

DOI: [10.1103/PhysRevLett.122.124302](https://doi.org/10.1103/PhysRevLett.122.124302)

In classical mechanics a massive particle accelerates in a potential linear in the coordinate. In quantum mechanics, the corresponding wave function accumulates not only a position-dependent phase, associated with this momentum change [1], but also a position-independent phase that scales with the third power of time [2]. In this Letter, we report on measurements of this cubic phase, predicted by Earle Hesse Kennard in 1927 for a Gaussian wave packet, by creating a linear potential for surface gravity water waves.

Phase contributions closely related to the Kennard phase emerge, for instance, in the Feynman path integral [3], the dispersionless free propagation of an Airy wave packet [4–6], the dynamics of neutrons in the gravitational field [7,8], the retroreflection of an atom laser beam from a potential barrier [9], and the interference of matter waves created [10–13] by a point source located in a linear potential. Despite this wide interest, no direct observation of the Kennard phase exists, since any setup measuring the probability density is insensitive to any global position-independent phase.

One way to circumvent this problem is to perform an interferometric measurement [14], e.g., with a path-dependent strength of the constant force [15]. However, our use of surface gravity water waves allows us to measure the full waveform providing us directly with the cubic phase.

In many aspects the time evolution of a wave function in quantum mechanics is analogous to that of paraxial optical beams [16], surface gravity water wave pulses [17–20], and underwater acoustic beams [21]. In this Letter, we utilize one of these analogies and study the propagation of surface gravity water waves in an effective linear potential, realized by a time-dependent homogeneous, and well-controlled

water flow. In particular, we focus on the evolution of Gaussian and Airy wave packets in this arrangement to gain insight into the corresponding quantum problem.

Both preserve the shape of their envelopes during propagation in a constant or linear potential. Indeed, a Gaussian wave packet spreads because of dispersion, but keeps its Gaussian shape. In contrast, the ideal Airy wave packet is “dispersion free,” that is it preserves its *exact* shape while it “self-accelerates” and follows a parabolic trajectory in space-time [4–6]. Moreover, a linear potential can change [22–26], and even eliminate [4,25–27] this self-acceleration, with the envelope of the Airy wave packet retaining its shape. These remarkable properties occur even for an exponentially truncated Airy wave packet [28].

For both Gaussian and Airy wave packets we experimentally confirm these predictions. Moreover, we measure directly the Kennard phase as well as its generalizations, and demonstrate that they crucially depend [15] on the initial profile of the wave packet.

For surface gravity water waves with low steepness moving in an external flow, the equation [29]

$$-i \frac{\partial A}{\partial \xi} = -\frac{\partial^2 A}{\partial \tau^2} - F\tau A \quad (1)$$

for the normalized amplitude envelope $A \equiv A(\tau, \xi)$ in the *comoving frame* has a form similar to the one-dimensional time-dependent Schrödinger equation of a particle in a linear potential $-F\tau$ corresponding to a constant “force” F .

However, the roles of time and space are interchanged. Indeed, the scaled dimensionless variables ξ and τ are

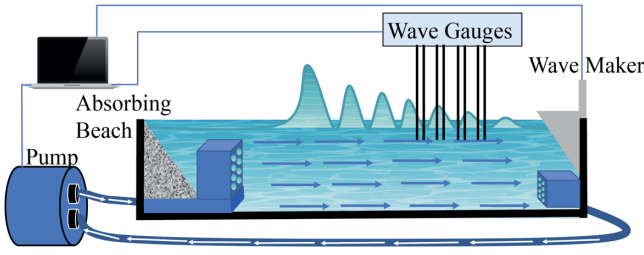


FIG. 1. Experimental setup for generating Gaussian and Airy surface gravity water wave packets moving in a time-dependent homogeneous flow created by a water pump.

related to the propagation coordinate x and the time t by $\xi \equiv \varepsilon^2 k_0 x$ and $\tau \equiv \varepsilon \omega_0 (x/c_g - t)$.

The carrier wave number k_0 and the angular carrier frequency ω_0 satisfy the deep-water dispersion relation $\omega_0^2 = k_0 g$, with g being the gravitational acceleration, and define the group velocity $c_g \equiv \omega_0/2k_0$. The parameter $\varepsilon \equiv k_0 a_0$ characterizing the wave steepness is assumed to be so small that Eq. (1) is free of nonlinear terms.

The complex amplitude envelope $A = |A| \exp(i\varphi_A)$ determines the variation in time and space of the surface elevation

$$\eta(t, x) \equiv a_0 |A(t, x)| \cos [k_0 x - \omega_0 t + \varphi_A(t, x)] \quad (2)$$

including the carrier wave, where a_0 is the maximum amplitude of the envelope.

The effective potential $-F\tau$ in Eq. (1) is determined [29] by the derivative $(\partial\Phi/\partial\tau)|_{Z=0}$ of the external dimensionless velocity potential $\Phi \equiv \phi/(\omega_0 a_0^2)$ at the free surface given by the dimensionless vertical coordinate $Z = 0$ with $Z \equiv \varepsilon k_0 z$. Hence, we can create the potential $F\tau \equiv 4\varepsilon(\partial\Phi/\partial\tau)|_{Z=0}$ by an externally operating water pump.

In order to measure the Kennard phase and its generalizations, we have conducted a series of experiments with surface gravity water waves moving in a time-dependent water flow shown in Fig. 1. The velocity of the homogeneous flow increases linearly in time and is induced by a computer-controlled water pump. Our experimental facility [30] allows us to generate flow velocities needed to observe this cubic phase. The water waves are generated by a computer-controlled wave maker [34] and measured by wave gauges.

The Gaussian envelope of the temporal surface elevation [35]

$$\eta^{(G)}(t, 0) \equiv a_0 \exp\left(-\frac{t^2}{t_0^2}\right) \cos(\omega_0 t) \quad (3)$$

prescribed by the wave maker at $x = 0$, with t_0 being the initial pulse size, gives rise to the Gaussian wave packet [15] with the amplitude

$$|A^{(G)}(\tau, \xi)| = \left(\frac{1}{1 + \xi^2/\xi_s^2}\right)^{1/4} \exp\left(-\frac{(\tau - F\xi^2)^2}{\tau_0^2(1 + \xi^2/\xi_s^2)}\right) \quad (4)$$

and the phase

$$\begin{aligned} \varphi_A^{(G)}(\tau, \xi) = & \frac{1}{2} \arctan\left(\frac{\xi}{\xi_s}\right) - \frac{\xi}{\xi_s} \frac{(\tau - F\xi^2)^2}{\tau_0^2(1 + \xi^2/\xi_s^2)} \\ & - F\tau\xi + \frac{F^2\xi^3}{3}, \end{aligned} \quad (5)$$

where $\tau_0 \equiv \varepsilon \omega_0 t_0$ and $\xi_s \equiv \tau_0^2/4$.

The first term in Eq. (5) determines the Gouy phase [36]. Moreover, we refer to the global phase cubic in ξ and quadratic in F expressed by the fourth term as the Kennard phase [2].

According to Eq. (4) the wave packet preserves its Gaussian shape while propagating along x , and its maximum follows a parabolic trajectory $t = x/c_g - (\varepsilon^3 k_0^2/\omega_0) F x^2$, which is the familiar manifestation of a constant ‘‘acceleration’’ with time and space interchanged. We confirm this property by measuring the elevations $\eta = \eta(t, x)$ of Gaussian wave packets at different locations x and times t without and with a linear growth of the water velocity, as depicted by black lines in Figs. 2(a) and 2(b), respectively.

In order to extract the trajectory of the wave packet in the laboratory frame, we obtain for each observed elevation η the mean value

$$\langle t \rangle(x) \equiv \frac{\int_{-\infty}^{+\infty} t |\eta(t, x)|^2 dt}{\int_{-\infty}^{+\infty} |\eta(t, x)|^2 dt} \quad (6)$$

of the temporal coordinate t as the function of x , shown in Fig. 2(c) by blue circles and red squares.

Next, we fit the expected parabolic dependence

$$\langle t \rangle(x) = a_1 x + a_2 x^2, \quad (7)$$

shown in Fig. 2(c) by blue and red curves (without and with external flow) to this data and obtain $a_1 = 2.82$ s/m, which is in good agreement with $c_g^{-1} = 2.86$ s/m, and $a_2 = 0.19$ s/m². This procedure yields $F \equiv -(\omega_0/\varepsilon^3 k_0^2) a_2 = -6.58$. Finally, the measured values of c_g and F lead to the blue and the red curves in Figs. 2(a) and 2(b) for the amplitude $|A^{(G)}|$, Eq. (4).

To measure the Kennard phase, we apply the Hilbert transform [30], and extract the phase $k_0 x - \omega_0 t + \varphi_A^{(G)}(t, x)$ of the surface elevation $\eta(t, x)$ at the maximum of the Gaussian amplitude $|A^{(G)}(t, x)|$, Eq. (4), that is along the line $\tau = F\xi^2$. After removing the carrier phase $k_0 x - \omega_0 t$, we present the remaining phase in Fig. 2(d) by blue circles (without external flow) and red squares (with external flow), together with the blue and red curves given by

$$\varphi_G(\xi) \equiv \varphi_A^{(G)}(\tau = F\xi^2, \xi) = \frac{1}{2} \arctan\left(\frac{\xi}{\xi_s}\right) - \frac{2}{3} F^2 \xi^3, \quad (8)$$

where we have used Eq. (5). We note that due to our experimental scheme of measuring at the maximum of the

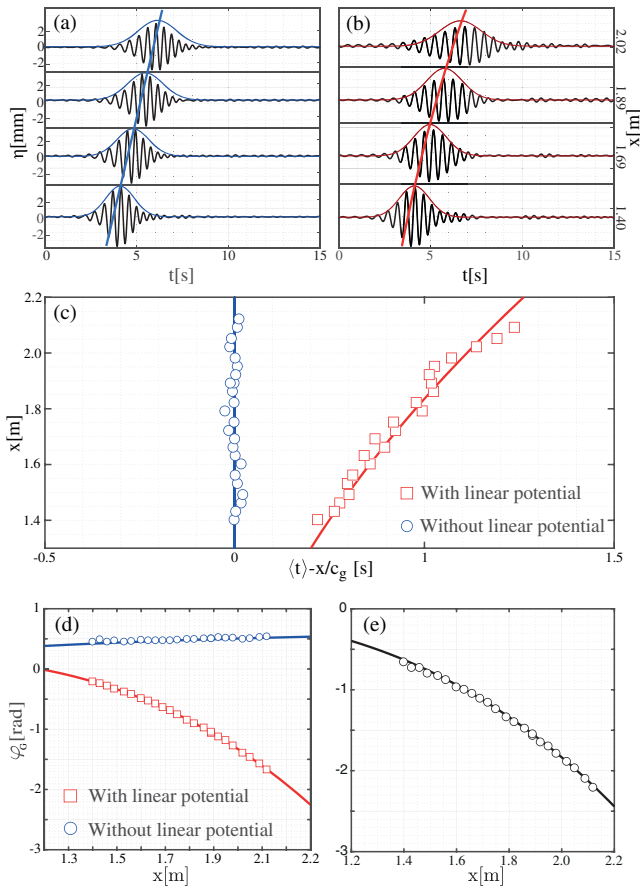


FIG. 2. Kennard phase for Gaussian surface gravity water wave packets. Observed surface elevation η (black line) and predicted envelopes (colored lines) given by Eqs. (2) and (4) without (a) and with (b) external flow. In both cases $k_0 = 20 \text{ m}^{-1}$, $a_0 = 5.0 \text{ mm}$ ($\varepsilon = 0.1$), $c_g = 0.35 \text{ m/s}$, and $t_0 = 0.72 \text{ s}$. The thick blue and red lines connect maxima of the envelopes measured for $x = 1.4 \text{ m}$, 1.69 m , 1.89 m , and 2.02 m . (c) The mean value $\langle t \rangle(x)$ (blue circles and red squares) of the temporal coordinate, Eq. (6). The corresponding solid lines are quadratic fits, Eq. (7), determining the group velocity $c_g = 1/a_1$ and the “force” $F \equiv -(\omega_0/\varepsilon^3 k_0^2)a_2 = -6.58$ in Eq. (1). (d) The phase offset of the Gaussian wave packet at its maximum without (blue circles) and with (red squares) external flow compared to the prediction by Eq. (8) represented by solid lines. (e) The modified Kennard phase, defined as the difference of the red squares and the blue circles presented in (d), with the black solid line given by $-(2/3)F^2\xi^3$, Eq. (8).

wave packet the coefficient of the Kennard phase has been changed from $1/3$ to $-2/3$.

Figure 2(d) clearly indicates that without the external flow ($F = 0$), only the Gouy phase manifests itself. When the external flow is applied ($F < 0$) the modified Kennard phase $-(2/3)F^2\xi^3$ appears, as shown in Fig. 2(e).

We emphasize that the Kennard phase, that is a global cubic phase, is not limited to a Gaussian wave packet but occurs for a wide variety of wave packets moving in a linear potential. Indeed, the solution

$$A(\tau, \xi) = \int_{-\infty}^{+\infty} G_F(\tau, \xi|\tau', 0)A(\tau', 0)d\tau' \quad (9)$$

of Eq. (1), which involves the initial envelope $A(\tau, 0)$ and the propagator [3]

$$G_F(\tau, \xi|\tau', 0) \equiv \frac{1}{2\sqrt{\pi\xi}} \exp\left(-iS_{cl}(\tau, \xi|\tau', 0) + i\frac{\pi}{4}\right) \quad (10)$$

with the classical action

$$S_{cl}(\tau, \xi|\tau', 0) \equiv \frac{(\tau - \tau')^2}{4\xi} + \frac{F\xi}{2}(\tau + \tau') - \frac{F^2}{12}\xi^3 \quad (11)$$

for a particle in a linear potential, contains the global cubic phase $F^2\xi^3/12$ proportional to the square of F .

Obviously, this term is closely related to the Kennard phase. However, as a result of the integration in the Huygens integral, Eq. (9), over τ' the phase cubic in ξ depends [15] also on the initial profile $A(\tau, 0)$. Indeed, we recall that for a Gaussian wave packet the prefactor is $1/3$ rather than $-1/12$.

We now study this generalized Kennard phase by extending our approach to Airy wave packets. The temporal surface elevation [37]

$$\eta^{(Ai)}(t, 0) \equiv a_0 \text{Ai}\left(-\frac{t}{t_0}\right) \exp\left(-\alpha\frac{t}{t_0}\right) \cos(\omega_0 t), \quad (12)$$

prescribed by the wave maker at $x = 0$, where t_0 and α denote the characteristic duration and the positive truncation parameter, gives rise to the Airy pulse with the amplitude

$$|A^{(Ai)}(\tau, \xi)| = |\text{Ai}\left\{\frac{1}{\tau_0}\left[\tau - \left(F + \frac{1}{\tau_0^3}\right)\xi^2\right] - 2i\alpha\frac{\xi}{\tau_0}\right\}| \times \exp\left[\alpha\frac{\tau}{\tau_0} - \alpha\left(F + \frac{2}{\tau_0^3}\right)\frac{\xi^2}{\tau_0}\right] \quad (13)$$

and the phase [30]

$$\varphi_A^{(Ai)}(\tau, \xi) = \left(\frac{F^2}{3} + \frac{F}{\tau_0^3} + \frac{2}{3\tau_0^6}\right)\xi^3 - \left(F + \frac{1}{\tau_0^3}\right)\tau\xi - \frac{\alpha^2}{\tau_0^2}\xi, \quad (14)$$

where $\tau_0 \equiv \varepsilon\omega_0 t_0$.

Equations (13) and (14) show [4] that the ideal Airy pulse, corresponding to $\alpha = 0$, exhibits three remarkable features: (i) it keeps its shape, (ii) its center-of-mass motion represents a parabola in the (τ, ξ) or (t, x) coordinates corresponding to the total “acceleration” $F + 1/\tau_0^3$, and (iii) it picks up cubic and linear phases in ξ .

We verify these properties by measuring the surface elevation $\eta = \eta(t, x)$ of regular ($t_0 < 0$) and inverted ($t_0 > 0$) Airy wave packets at different locations x and

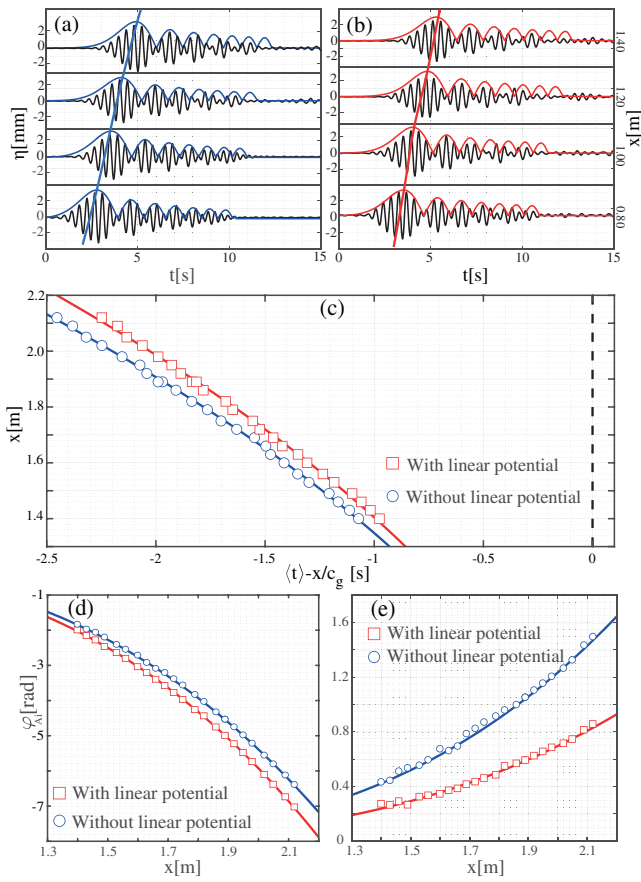


FIG. 3. Generalized Kennard phase for inverted Airy surface gravity water wave packets. Observed surface elevation η (black line) and predicted envelopes (colored lines) given by Eqs. (2) and (13) without (a) and with (b) external flow. In both cases $k_0 = 23 \text{ m}^{-1}$, $a_0 = 3.93 \text{ mm}$ ($\varepsilon = 0.09$), $c_g = 0.33 \text{ m/s}$, $t_0 = 0.82 \text{ s}$, and $\alpha = 0.05$. The thick blue and red lines connect maxima of the envelopes measured for $x = 0.8 \text{ m}$, 1.0 m , 1.2 m , and 1.4 m . (c) The mean value (blue circles and red squares) of the temporal coordinate $\langle t \rangle(x)$, defined by Eq. (6), with integration performed only over the main lobe, is determined by the surface elevation η for the parameter $t_0 = 0.27 \text{ s}$. The corresponding solid lines are quadratic fits, Eq. (7), determining $c_g = 1/a_1$ together with $F + 1/\tau_0^3 \equiv -(\omega_0/\varepsilon^3 k_0^2) a_2$ and thus $F = -1.94$. The black dashed line $x = c_g t$ is shown for comparison. (d) The phase offset of the Airy wave packet at the maximum of the main lobe without (blue circles) and with (red squares) external flow, the solid lines are given by Eq. (15). (e) The generalized Kennard phase, obtained by subtracting the linear terms $(F + 1/\tau_0^3)\tau\xi$ and $(\alpha^2/\tau_0^2)\tau\xi$, Eq. (14), at $\tau = \tau_{\max}^{(Ai)}(\xi)$ from the total measured phase presented in (d). The blue and red curves represent the theoretical predictions, $2\xi^3/(3\tau_0^6)$ and $[F^2/3 + F/\tau_0^3 + 2/(3\tau_0^6)]\xi^3$, accordingly.

times t without and with an external flow. These measurements are presented in [30] and in Fig. 3, respectively.

The black lines in Figs. 3(a) and 3(b) verify that indeed the Airy pulse preserves its envelope while propagating in a constant ($F = 0$) [17], and in a linear potential ($F < 0$).

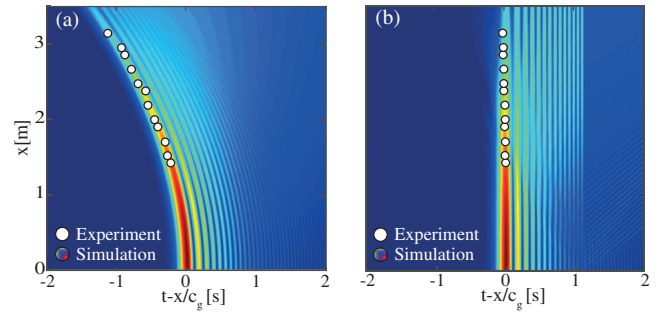


FIG. 4. Cancellation of the self-acceleration of an inverted Airy wave packet by a linear potential. Experimental results (white dots) and simulations (colored density plot) based on Eq. (1), for an inverted Airy wave packet without (a) and with (b) an external flow, corresponding to $F = 0$ and $F = -11.38$, accordingly. In both cases $k_0 = 23 \text{ m}^{-1}$, $a_0 = 3 \text{ mm}$ ($\varepsilon = 0.07$), $t_0 = 0.32 \text{ s}$, $\alpha = 0.05$, and $c_g = 0.33 \text{ m/s}$.

In Fig. 3(c) we present by blue circles (without flow) and red squares (with flow) the location of the main lobe versus the mean time $\langle t \rangle$, defined by Eq. (6), with the integration performed only over the main lobe. For the comparison with the theoretical predictions, we fit in Fig. 3(c) to this data the expected parabolic dependence of $\langle t \rangle$, Eq. (7), and obtain without flow $a_1 = 3.03 \text{ s/m}$ and $a_2 = -0.55 \text{ s/m}^2$, in good agreement with $a_1 = c_g^{-1} = 3.05 \text{ s/m}$, and $a_2 = -k_0^2/(\omega_0^4 t_0^3) = -0.55 \text{ s/m}^2$. With flow, we find $a_1 = 3.03 \text{ s/m}$ and $a_2 = -0.5 \text{ s/m}^2$ as shown by the red solid line in Fig. 3(c), resulting in the dimensionless parameter $F = -1.94$.

Next, we apply the Hilbert transform [30] to extract [38] the phase variation $k_0 x - \omega_0 t + \varphi_A^{(Ai)}(t, x)$ of the surface elevation $\eta(t, x)$, Eq. (2), at the maximum of the main lobe, that is along the line $\tau = \tau_{\max}^{(Ai)}(\xi) \equiv \tau_{\max}^{(Ai)}(0) + (F + 1/\tau_0^3)\xi^2$. Here, $\tau_{\max}^{(Ai)}(0)$ denotes the position of the maximum of the main lobe for $\xi = 0$.

After removing the carrier phase $k_0 x - \omega_0 t$, we present the remaining phase in Fig. 3(d) by blue circles (without flow) and red squares (with flow), together with the blue and red lines given by

$$\varphi_{Ai}(\xi) \equiv \varphi_A^{(Ai)}[\tau = \tau_{\max}^{(Ai)}(\xi), \xi]. \quad (15)$$

In contrast to the Gaussian wave packets, the Airy ones have cubic phase terms $2\xi^3/(3\tau_0^6)$ even in the absence of a linear potential ($F = 0$) as shown by Eq. (14). Since an Airy wave packet is a multipeak function, we subtract the linear term $(F\tau + \tau/\tau_0^3 + \alpha^2/\tau_0^2)\xi$ with $\tau = \tau_{\max}^{(Ai)}(\xi)$ from the total measured phase, displayed in Fig. 3(d). We present the corresponding results for the cubic contributions in Fig. 3(e) together with the theoretical predictions $2\xi^3/(3\tau_0^6)$ (without flow) and $[F^2/3 + F/\tau_0^3 + 2/(3\tau_0^6)]\xi^3$ (with flow) shown by blue and red curves.

We conclude by demonstrating that a linear potential can cancel [4,39] the self-acceleration of the Airy wave packets. Indeed, as depicted in Fig. 4, the parabolic trajectory (a) of the main lobe becomes linear (b), that is it starts to propagate with the group velocity c_g . Moreover, in contrast to Gaussian wave packets, which spread in a linear potential, Fig. 2(b), Airy wave packets preserve their shapes, since they are solutions [1,9] of the stationary Schrödinger equation with a linear potential.

In conclusion, we have observed Gaussian and Airy surface gravity water wave packets moving in an effective linear potential obtained by operating a water pump. Moreover, we have derived theoretically, and measured successfully the Kennard phase and its generalizations, [2–4] for Gaussian and Airy wave packets. Finally, we have demonstrated the cancellation [4] of the self-acceleration of the Airy surface gravity water wave packets.

We emphasize that our experimental setup is neither limited to Gaussian and Airy wave packets, nor to a linear potential. Indeed, it allows us to study the time evolution of an arbitrary wave packet in a wide variety of potentials. Moreover, by exciting wave packets with higher steepness in the water tank, nonlinear terms of the wave equation come into play, enabling us to study the evolution of amplitude and phase under the combined effects of the potential and the nonlinearity [40,41].

We thank A. Chernyshova and E. Ginzburg for fruitful discussions, and Tamir Ilan for technical support and advice. This work is supported by the German-Israeli Project Cooperation DIP (Project No. AR 924/1-1, DU 1086/2-1), the Israel Science Foundation (Grant No. 1415/17), and the Israel Ministry of Science, Technology and Space (Grant No. 3-12473). M. A. E. is thankful to the Center for Integrated Quantum Science and Technology (IQST) for its generous financial support. W. P. S. is grateful to Texas A & M University for support through a Faculty Fellowship at the Hagler Institute for Advanced Study at the Texas A & M University as well as to the Texas A & M AgriLife Research. The research of the IQST is financially supported by the Ministry of Science, Research and Arts Baden-Württemberg.

[1] D. J. Griffiths, *Introduction to Quantum Mechanics*, 2nd ed. (Cambridge University Press, Cambridge, England, 2017).
 [2] E. H. Kennard, *Z. Phys.* **44**, 326 (1927); *J. Franklin Inst.* **207**, 47 (1929).
 [3] R. P. Feynman and A. R. Hibbs, *Quantum Mechanics and Path Integrals* (McGraw-Hill, New York, USA, 1965).
 [4] M. V. Berry and N. L. Balazs, *Am. J. Phys.* **47**, 264 (1979).
 [5] D. M. Greenberger, *Am. J. Phys.* **48**, 256 (1980).
 [6] E. Kajari, N. L. Harshman, E. M. Rasel, S. Stenholm, G. Süssmann, and W. P. Schleich, *Appl. Phys. B* **100**, 43 (2010).
 [7] V. V. Nesvizhevsky, H. G. Börner, A. K. Petukhov, H. Abele, S. Baeßler, F. J. Rueß, T. Stöferle, A. Westphal,

A. M. Gagarski, G. A. Petrov, and A. V. Strelkov, *Nature (London)* **415**, 297 (2002).
 [8] T. Jenke, G. Cronenberg, J. Burgdörfer, L. A. Chizhova, P. Geltenbort, A. N. Ivanov, T. Lauer, T. Lins, S. Rotter, H. Saul, U. Schmidt, and H. Abele, *Phys. Rev. Lett.* **112**, 151105 (2014).
 [9] M. Köhl, Th. W. Hänsch, and T. Esslinger, *Phys. Rev. Lett.* **87**, 160404 (2001).
 [10] Yu. N. Demkov, V. D. Kondratovich, and V. N. Ostrovskii, *Pis'ma Zh. Eksp. Theor. Fiz.* **34**, 425 (1981) [*JETP Lett.* **34**, 403 (1981)].
 [11] M. V. Berry, *J. Phys. A* **15**, L385 (1982).
 [12] C. Blondel, C. Delsart, and F. Dulieu, *Phys. Rev. Lett.* **77**, 3755 (1996).
 [13] C. Nicole, H. L. Offerhaus, M. J. J. Vrakking, F. Lépine, and Ch. Bordas, *Phys. Rev. Lett.* **88**, 133001 (2002).
 [14] F. Fratini and L. Safari, *Phys. Scr.* **89**, 085004 (2014).
 [15] M. Zimmermann, M. A. Efremov, A. Roura, W. P. Schleich, S. A. DeSavage, J. P. Davis, A. Srinivasan, F. A. Narducci, S. A. Werner, and E. M. Rasel, *Appl. Phys. B* **123**, 102 (2017).
 [16] M. Born and E. Wolf, *Principles of Optics* (Cambridge University Press, Cambridge, England, 2002).
 [17] S. Fu, Y. Tsur, J. Zhou, L. Shemer, and A. Arie, *Phys. Rev. Lett.* **115**, 034501 (2015).
 [18] S. Fu, Y. Tsur, J. Zhou, L. Shemer, and A. Arie, *Phys. Rev. Lett.* **115**, 254501 (2015).
 [19] S. Fu, Y. Tsur, J. Zhou, L. Shemer, and A. Arie, *Phys. Rev. E* **93**, 013127 (2016).
 [20] M. V. Berry, R. G. Chambers, M. D. Large, C. Upstill, and J. C. Walmsley, *Eur. J. Phys.* **1**, 154 (1980).
 [21] U. Bar-Ziv, A. Postan, and M. Segev, *Phys. Rev. B* **92**, 100301 (2015).
 [22] N. K. Efremidis, *Opt. Lett.* **36**, 3006 (2011).
 [23] Z. Ye, S. Liu, C. Lou, P. Zhang, Y. Hu, D. Song, J. Zhao, and Z. Chen, *Opt. Lett.* **36**, 3230 (2011).
 [24] F. Bleckmann, A. Minovich, J. Frohnhaus, D. N. Neshev, and S. Linden, *Opt. Lett.* **38**, 1443 (2013).
 [25] Z. Ye, S. Liu, C. Lou, P. Zhang, Y. Hu, D. Song, J. Zhao, and Z. Chen, *Opt. Lett.* **36**, 3230 (2011).
 [26] S. Chavez-Cerda, U. Ruiz, V. Arrizn, and H. M. Moya-Cessa, *Opt. Express* **19**, 16448 (2011).
 [27] W. Liu, D. N. Neshev, I. V. Shadrivov, A. E. Miroshnichenko, and Y. S. Kivshar, *Opt. Lett.* **36**, 1164 (2011).
 [28] G. A. Siviloglou, J. Broky, A. Dogariu, and D. N. Christodoulides, *Phys. Rev. Lett.* **99**, 213901 (2007).
 [29] C. C. Mei, *The Applied Dynamics of Ocean Surface Waves* (Wiley-Interscience, New York, USA, 1983).
 [30] See Supplemental Material at <http://link.aps.org/supplemental/10.1103/PhysRevLett.122.124302> for the experimental setup, a description of the Hilbert transform, the complete phase expression for truncated Airy wave packets, error estimates, and the measurements of regular Airy wave packets, which includes Refs. [31–33].
 [31] L. Shemer, K. Goulitski, and E. Kit, *Eur. J. Mech. B* **26**, 193 (2007).
 [32] F. W. King, *Hilbert Transforms* (Cambridge University Press, Cambridge, England, 2009), Vol. 1.

- [33] A documentation of the Matlab toolbox function “hilbert” is provided at <https://www.mathworks.com/help/signal/ug/hilbert-transform.html>.
- [34] We emphasize that the computer-controlled wave maker can generate any initial wave profile. In contrast to optics, where a phase mask (or lens) is usually used to create Airy wave packets, there is no need for such a device in the case of water waves.
- [35] The initial Gaussian profile of the amplitude envelope reads $A^{(G)}(\tau, 0) = \exp(-\tau^2/\tau_0^2)$.
- [36] S. Feng and H. G. Winful, *Opt. Lett.* **26**, 485 (2001).
- [37] The initial profile of the amplitude envelope for the Airy pulse reads $A^{(Ai)}(\tau, 0) = \text{Ai}(\tau/\tau_0) \exp(\alpha\tau/\tau_0)$.
- [38] The phase $2\xi^3/(3\tau_0^6)$ for a freely propagating Airy wave packet has been measured [17] recently in a range from zero rads to 120 rads. Since the phase accumulated between measurement points exceeded 2π , it was assumed to be monotonic. However, the measurement reported here does not require this assumption on the phase steps between measurements, since the entire measurement range is limited to the interval $[0, 2\pi]$.
- [39] We emphasize that so far only Airy beams propagating in an optically induced refractive-index potential [23] and plasmonic Airy beams [24] have allowed an experimental control of their accelerations.
- [40] H. H. Chen and C. S. Liu, *Phys. Rev. Lett.* **37**, 693 (1976).
- [41] V. N. Serkin, A. Hasegawa, and T. L. Belyaeva, *Phys. Rev. Lett.* **98**, 074102 (2007).